To cite this version :

Olivier CASTELNAU, Ricardo LEBENSOHN, Pedro Ponte CASTAEDA, Donna BLACKMAN - Earth Mantle Rheology Inferred from Homogenization Theories, chapitre 4 - 2008

Earth Mantle Rheology Inferred from Homogenization Theories

4.1. Introduction

The Earth's upper mantle is known to exhibit elastic anisotropy, which is commonly attributed to the presence of Lattice Preferred Orientations (LPO). Such anisotropy is revealed in recordings of seismic waves that travel through the mantle with speeds that depend on propagation and/or polarization direction. The development of LPO is due to the plastic deformation of mantle minerals associated with large-scale convective flow. Both olivine and pyroxene crystals exhibit an orthorhombic structure and have only a few slip systems available for dislocation creep. This leads to very high viscoplastic anisotropy at the grain scale, so that an upper mantle region with strong seismic anisotropy (i.e., pronounced LPO) may also exhibit a large effective viscoplastic anisotropy which may manifest itself as differences in effective viscosities of up to one or two orders of magnitude depending on the loading direction. This may have a large influence on the flow in (at least) some regions of the mantle [CHR 87], as was also shown for the flow of ice in ice sheets [MAN 97], but the topic has received little attention [BLA 07]. The key of this issue is to understand the link between single crystal rheology, microstructure (in particular LPO) and associated polycrystal behavior, e.g. as attempted for polar ices [CAS 08b].

In this study, the impact of LPO on mantle rheological properties is assessed using numerical investigation of the viscoplastic behavior of olivine $(Mg,Fe)_2SiO_4$. This mineral constitutes the major proportion ($\sim 60\%$) of the upper mantle. Olivine

rheology, under pressure and temperature conditions relevant for the upper mantle (typically 10GPa, 1500°C), is complex, see [KAR 93, HIR 03] for a review. Dislocation and diffusion creep regimes may be encountered at different depths, but only the former regime is considered here. Basically, the plastic behavior is strongly influenced by the pressure which leads to an inversion of the hard and soft slip systems [DUR 05, RAT 07], the water fugacity [MAC 85], the presence of melt pockets [KOH 96]. Dynamic recrystallization also significantly affects LPO evolution at large strain [ZHA 95]. Note finally that twinning is not a known deformation mechanism for olivine.

A challenging feature in olivine plasticity is the lack of five independent slip systems at the grain level, which, according to the von Mises criterion, are necessary to accommodate arbitrary plastic deformation. According to [WEN 99, TOM 00], the tangent (TGT) Self-Consistent (SC) polycrystal model predicts a finite flow stress with only three independent systems, which is a puzzling result. It is however worth noting that hexagonal polycrystals with only basal and prismatic slips, i.e. with four independent systems, are found to be able to deform plastically [HUT 77, NEB 00]. However, according to [NEB 01], this result is model dependent. A systematic recent study based on full-field modeling [LEB 07] has shown that, effectively, three independent systems are not sufficient for olivine polycrystals (see also [CAS 08a]).

Several polycrystal plasticity mean-field (homogenization) models have been applied to olivine aggregates, generally to assess LPO evolution and much more rarely to investigate their (*non-linear*) rheological behavior. In addition to the classical uniform stress (static) bound used by [CHA 93, DAW 00], several models have been constructed to deal specifically with crystals lacking five (even four) independent slip systems [PAR 90, KAM 01], the latter being employed in a number of recent geophysical applications. The tangent extension of the Self-Consistent (SC) scheme [MOL 87, LEB 93], generally referred to as the "VPSC model" in the geophysical literature, has often been described as if the interaction between each grain and its surrounding could be approximated by the interaction between one ellipsoidal grain with the same lattice orientation as the original grain and a homogenous equivalent medium whose behavior represents that of the polycrystal, thus taking advantage of the analytical solution of [ESH 57] for the inclusion/matrix interaction. This reasoning led to the conclusion that the TGT scheme fulfils the implicit assumption of uniform stress and strain-rate inside the grains, which is not correct (see [PON 98] for a review). More recently, as for the extensions of the SC scheme for polycrystals exhibiting non-linear rheology, the variational estimate [PON 91, BOT 95] and the second order (SO) procedure [PON 02, LIU 04] have provided major improvements. Both of them exhibit very interesting features, such as the prediction of effective potentials lying beneath rigorous upper bounds generally violated by other homogenization procedures [GIL 95]. Following [PON 96, MAS 00] further proposed the "affine extension" (AFF), which can be also seen as a rather crude approximation of the SO procedure.

Basically, all these methods are based on the definition of an "N-Phase Linear Comparison Polycrystal" (NPLCP) having the same microstructure as the real non-linear polycrystal and to which the SC scheme (originally developed for materials exhibiting *linear* behavior [HER 54, KRÖ 58]) can be applied in order to obtain the behavior of the real polycrystal. The number of models proposed in the literature turns out to be significant, reflecting the difficulty of finding the optimal NPLCP. In addition to these mean-field estimates, full-field approaches have been proposed to calculate the fluctuation of the stress and strain-rate inside grains, together with the overall poly-crystal behavior. The results given by these approaches can be considered "exact" (or at least reference) solutions. In this context, a numerically efficient method based on Fast Fourier Transforms (FFT) has been proposed [MOU 98] and applied to polycrys-tals [LEB 01]. We will see that this method is very helpful to understand the details of the material response and to assess the validity of mean-field estimates.

The aim of this paper is to provide new insight into the rheology of olivine poly-crystals. We focus on the lack of five independent slip systems, its impact on the effec-tive behavior and on the stress and strain-rate distributions inside individual grains. This work is limited to the study of the *instantaneous* flow stress of *isotropic* (random LPO) polycrystals. We consider a simple but realistic rheology at the grain scale (sec-tion 4.2). Reference results obtained by the full-field approach based on the FFT pro-cedure are presented (section 4.3) and compared to estimates provided by mean-field approaches (section 4.4), followed by several concluding observations (section 4.5).

4.2. Grain local behavior

At the grain (local) scale, we consider deformation that occurs only by dislocation creep on a given number of slip systems. The resolved shear stress $\tau_{(k)}$ acting on a slip system (k) is given by a projection of the local deviatoric stress tensor $\boldsymbol{\sigma}$

$$\tau_{(k)}(\mathbf{x}) = \boldsymbol{\mu}_{(k)}^{(r)} : \boldsymbol{\sigma}(\mathbf{x}) \qquad [4.1]$$

with $\boldsymbol{\mu}_{(k)}^{(r)}$ the Schmid tensor expressing the orientation of the slip system with respect to a laboratory reference frame and (r) representing the crystal orientation at a given spatial position $\mathbf{x}$. As for the constitutive relation at the slip system level, we use a classical power law for the slip rate $\dot{\gamma}$ on system (k)

$$\dot{\gamma}_{(k)}(\mathbf{x}) = \dot{\gamma}_0 \left| \frac{\tau_{(k)}(\mathbf{x})}{\tau_{0(k)}} \right|^{n_{(k)}-1} \frac{\tau_{(k)}(\mathbf{x})}{\tau_{0(k)}} \qquad [4.2]$$

with $\tau_{0(k)}$ the reference shear stress of the system (k), $n_{(k)}$ the corresponding stress sensitivity and $\dot{\gamma}_0$ a reference slip rate. Combining all available slip systems, the local

$$\dot{\varepsilon}(\mathbf{x}) = \sum_{k=1}^{K} \boldsymbol{\mu}_{(k)}^{(r)} \dot{\gamma}_{(k)}(\mathbf{x}) \qquad\qquad [4.3]$$

with K the total number of slip systems.

The dislocation slip systems considered here are those used by [TOM 00] based on several sets of experimental results. They are listed in the *first seven lines* of Table 4.1 and illustrated in Figure 4.1. Easy slip occurs in olivine along the $[100]$ direction, whereas slip along the $[001]$ direction is permitted, but with a higher resistance. These conditions are appropriate for "dry" crystals deformed at high temperature and low pressure. We have chosen the same stress sensitivity $n_{(k)} = n = 3.5$ for all systems, a tendency that appears to be supported by the experimental data. Typical values for τ_0 and $\dot{\gamma}_0$ for conditions prevailing in the upper mantle are $\sim$ 1MPa and $\sim 10^{-15} s^{-1}$, respectively. Only three of these slip systems are independent. They allow shearing of the crystal lattice, but none of them allow axial deformation along the $\mathbf{a}$, $\mathbf{b}$ or $\mathbf{c}$ lattice directions. Consequently, these systems cannot accommodate an arbitrary plastic deformation of olivine crystals. Following the generally adopted procedure (see e.g. [TOM 00, WEN 99]), we introduce an additional ("cubic like") slip

Slip system	# equiv.	$\tau_{0(k)}$
$(010)[100]$	1	τ_0
$(001)[100]$	1	τ_0
$(010)[001]$	1	$2\tau_0$
$(100)[001]$	1	$3\tau_0$
$\{011\}[100]$	2	$4\tau_0$
$\{031\}[100]$	2	$4\tau_0$
$\{110\}[001]$	2	$6\tau_0$
$\{111\}\langle 1\bar{1}0\rangle$	12	$M_1\tau_0$
$\{101\}\langle \bar{1}01\rangle$	2	$M_2\tau_0$

Table 4.1. *Slip plane (hkl) and orientation of the Burgers vector $[uvw]$ considered for olivine grains, together with the number of equivalent systems for each family (k) and the reference shear stresses $\tau_{0(k)}$. The first 7 families have been observed experimentally. The "cubic like" system $\{111\}\langle 1\bar{1}0\rangle$ is added for the sake of having 5 independent slip systems at the grains scale; it comprises 12 systems that are not exactly equivalent owing to the orthorhombic structure of olivine crystals, but this distinction has not been considered here. The last system $\{101\}\langle \bar{1}01\rangle$ comprises two slip planes and slip directions*
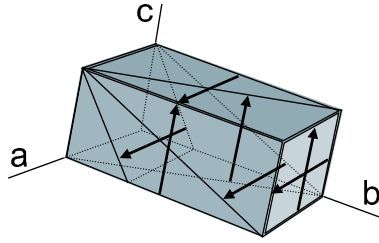
Figure 4.1. *Schematic representation of observed slip systems in olivine single crystals*

family $\{111\}\langle 1\bar{1}0\rangle$ the resistance of which is expressed by the scalar M_1, for the purpose of having five independent systems available at the crystal level (Table 4.1). We further introduce a last set of slip systems, $\{101\}\langle \bar{1}01\rangle$, which activation allows axial straining of the crystal lattice along **a** and **c** (but not along **b**), a way to mimic somehow the deformation that dislocation climb would produce. The resistance of these last systems is given by M_2. In the following, we will focus on the effect of M_1 and M_2 on the effective behavior and on the stress and strain-rate heterogenities within the polycrystal. Playing with M_1 and M_2, we can investigate materials with 3, 4 and 5 independent slip systems. Evidently, the limiting cases $M_i \to \infty$ are equivalent to removing the corresponding set of systems, leaving the grain with infinite normal viscosities along some of the **a**, **b** and **c** directions and an open yield surface. The procedure followed here will allow us to assess the relevance of different homogenization methods for olivine and to shed light on the local mechanical state of olivine polycrystals deforming in the dislocation creep regime. In a forthcoming study, we will replace the two last slip systems M_1 and M_2 by appropriate physically-based accommodation processes (climb, grain boundary sliding, etc.) but this requires further theoretical developments.

4.3. Full-field reference solutions

Full-field reference results are obtained with the FFT method [MOU 98, LEB 01] which consists of finding a strain-rate field associated with a kinematically admissible velocity field that minimizes the average local work rate under the compatibility and equilibrium constraints. A regular Fourier grid of $64 \times 64 \times 64$ points has been used to discretize the periodic 3D unit-cells, randomly generated by Voronoi tessellation and containing 32 randomly oriented grains (Figure 4.2). To ensure the statistical relevance of the results, a total average has been performed over 50 of those random configurations. The mechanical behavior calculations were performed for uniaxial compression with an equivalent macroscopic strain-rate $\dot{\bar{\varepsilon}}_{eq} = \dot{\gamma}_0$, with $\dot{\bar{\varepsilon}}_{eq} = \sqrt{2/3\dot{\bar{\varepsilon}} : \dot{\bar{\varepsilon}}}$ and $\dot{\bar{\varepsilon}}$ denoting the macroscopic strain-rate tensor. In this section and in the beginning of the next one, calculations have been performed with $M_2 \to \infty$, so that crystals are left with only 3 independent slip systems as $M_1 \to \infty$ (and 5 for finite values of M_1).
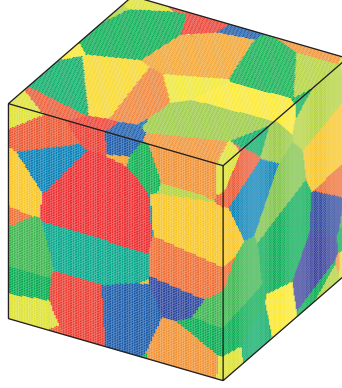
Figure 4.2. *Typical periodic microstructure generated by Voronoi tesselation. It contains 32 grains, each having a different color corresponding to its crystallographic orientation*

Full-field approaches can be used advantageously to examine the distribution of the stress and strain-rate within the microstructure. A 3D overview of the distribution of the local equivalent stress $\sigma_{eq}(\mathbf{x})$ and strain-rate $\dot{\varepsilon}_{eq}(\mathbf{x})$ is given in Figure 4.3 for $M_1 = 10$ and $M_1 = 100$, with $\sigma_{eq}(\mathbf{x}) = \sqrt{3/2\boldsymbol{\sigma}(\mathbf{x}) : \boldsymbol{\sigma}(\mathbf{x})}$ and $\dot{\varepsilon}_{eq}(\mathbf{x}) = \sqrt{2/3\dot{\boldsymbol{\varepsilon}}(\mathbf{x}) : \dot{\boldsymbol{\varepsilon}}(\mathbf{x})}$. It can be seen that strong stress and strain-rate localization occurs, with concentrations in bands located either within the grains or lying along grain boundaries, whereas higher values are found at grain boundaries. Also clearly observed is the drastic effect of M_1, with increasing stress and strain-rate heterogeneities observed at high M_1 values, corresponding to grains that can be hardly deformed axially along **a**, **b** and **c** lattice directions.

To evaluate this feature more quantitatively, we have plotted in Figure 4.4 the value of $\dot{\varepsilon}_{eq}(\mathbf{x})$ against that of $\sigma_{eq}(\mathbf{x})$, for each Fourier point of one of the 50 random FFT configurations. An average of $64^3/32 = 8192$ dots are thus plotted for each grain, i.e. enough for a statistical representation of the intragranular field heterogenity. No clear trend is to be found in those plots. The local equivalent strain-rate can be high (or low) with either a low or high local stress level, depending on the spatial position $\mathbf{x}$ of the observation point. There is globally no correlation between *local* $\sigma_{eq}(\mathbf{x})$ and $\dot{\varepsilon}_{eq}(\mathbf{x})$ values and this expresses the tremendous effect of the intergranular interactions: the local mechanical state in the material is not only guided by the local crystallographic orientation of the considered grain, but it is also highly influenced by the neighborhood. Therefore, the microstructure cannot be described as consisting of "hard" and "soft" grains depending of their orientation, as sometimes proposed in the literature. However, as shown by [CAS 08a], *phase average* values[1] $\sigma_{eq}^{(r)}$ and $\dot{\varepsilon}_{eq}^{(r)}$ are correlated,

---

1. The phase average is the average value over a large (i.e. statistically relevant) number of grains exhibiting the same crystallographic orientation.
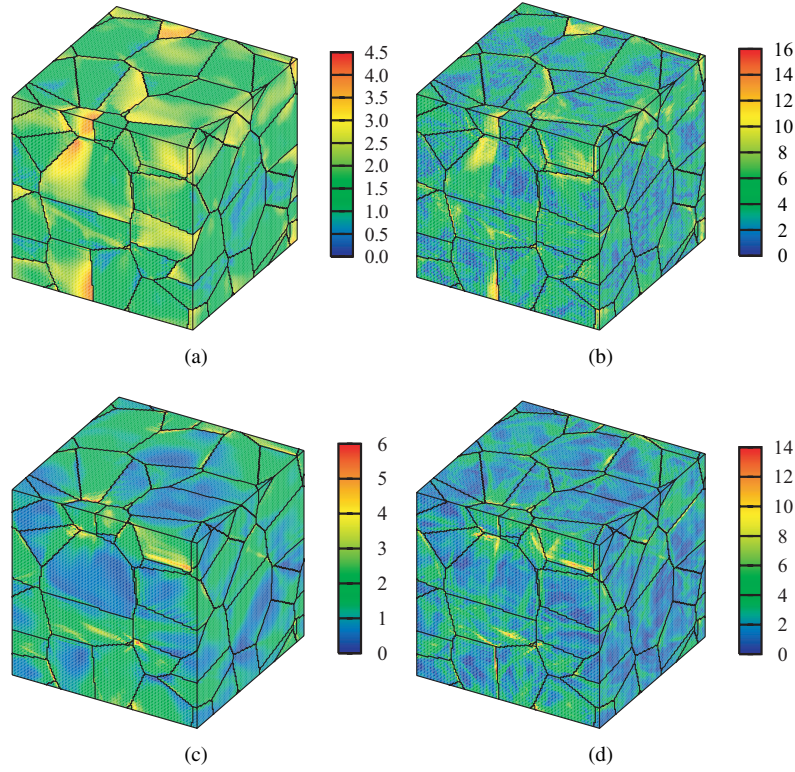
Figure 4.3. *Spatial distribution of (a,b) $\sigma_{eq}/\bar{\sigma}_{eq}$ and (c,d) $\dot{\varepsilon}_{eq}/\dot{\bar{\varepsilon}}_{eq}$ calculated by the FFT method for (a,c) $M_1 = 10$ and (b,d) $M_1 = 100$, for the microstructure given in Figure 4.2. Solid lines indicate the grain boundaries (and cube edges). The direction of uniaxial tension is vertical. Note the different scales for each figure*

with low average (equivalent) stress and high average (equivalent) strain-rate for the "soft" orientations and the reverse situation for the "hard" orientations. The corollary of this feature is that, for the experimental characterization of active deformation mechanisms by e.g. electron microscopy, a very large number of grains with a similar orientation have to be observed if we want to attain statistically representative conclusions. It should also be emphasized that $\sigma_{eq}(\mathbf{x})$ and $\dot{\varepsilon}_{eq}(\mathbf{x})$ are generally much larger than their macroscopic counterpart $\bar{\sigma}_{eq}$ and $\dot{\bar{\varepsilon}}_{eq}$, in particular at high M_1, as also shown in Figure 4.3. A material point is thus submitted to much more stringent mechanical conditions than the average polycrystal, a feature that has to be taken into account when using single crystal data to infer polycrystal behavior.
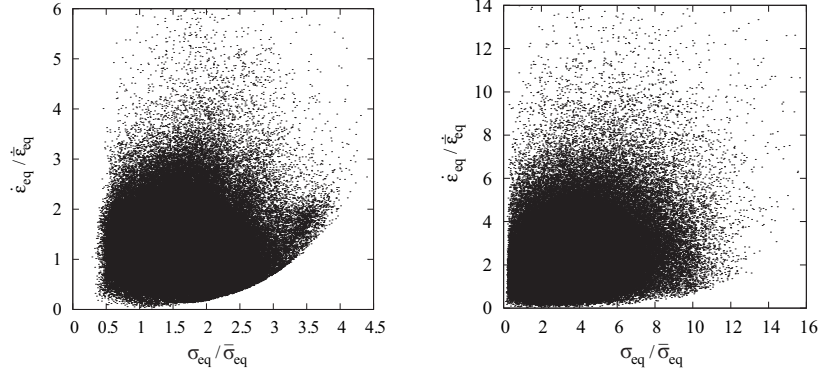
Figure 4.4. *Relation between $\dot{\varepsilon}_{eq}/\dot{\bar{\varepsilon}}_{eq}$ and $\sigma_{eq}/\bar{\sigma}_{eq}$ for each Fourier points of the microstructure shown above, for (left) $M = 10$ and (right) $M = 100$. Note the different scales*

4.4. Mean-field estimates

4.4.1. *Basic features of mean-field theories*

Unlike full-field solutions, the aim of mean-field theories is to provide bounds or estimates of the polycrystal effective response without having to evaluate the details of local fields. Consequently, these methods present the advantage of a very low computational cost, as compared to full-field methods, enabling their eventual coupling with large scale flow models such as regional or global convection models of the Earth. Here, we are limited to a statistical description of the microstructure; that is, the precise location of each grain is not known, but only the main geometrical features of the microstructure (e.g. isotropic distribution of grains, etc.) are supposed. Field distributions are thus out of reach. As for the SC scheme, well adapted for polycrystal, only the first and second order moments of the stress and strain-rate (respectively $\boldsymbol{\sigma}^{(r)} = \langle \boldsymbol{\sigma} \rangle^{(r)}$ and $\langle \boldsymbol{\sigma} \otimes \boldsymbol{\sigma} \rangle^{(r)}$ and similarly for the strain-rate) are available, e.g. see [PON 98]. The real difficulty for mean-field approaches is to capture the effect of the field heterogeneities (evidenced in the previous section) on the effective behavior, without completely evaluating those heterogeneities. According to the preceding section, this might become increasingly challenging as M_1 increases.

We will not detail here the theoretical background of the different mean-field methods proposed in the literature, but only the very basic features will be reviewed. The reader is referred to the relevant publications for more details. As already indicated, the SC scheme provides an exact solution for some specific random polycrystal microstructures, but only in the context of *linear* local behavior (e.g. linear thermo-elasticity). For *non-linear* behavior as considered here, the usual treatment consists of defining a *linear* comparison material (the NPLCP) exhibiting *phase uniform* compliances and stress-free (or thermal) strain-rates so that it can be homogenized by the

(linear) SC scheme. The fields in the non-linear polycrystal of interest generally do not identify exactly with those of the NPLCP [IDI 07]. Generally speaking, the linearization of [4.2] can be expressed in the form

$$\dot{\gamma}_{(k)}(\mathbf{x}) = \alpha_{(k)}^{(r)} \tau_{(k)}(\mathbf{x}) + \dot{e}_{(k)}^{(r)} \qquad [4.4]$$

with the shear compliance $\alpha_{(k)}^{(r)}$ and stress-free shear-rate $\dot{e}_{(k)}^{(r)}$ depending on two reference shear stresses, $\check{\tau}_{(k)}^{(r)}$ and $\hat{\tau}_{(k)}^{(r)}$

$$\alpha = \frac{\dot{\gamma}(\hat{\tau}) - \dot{\gamma}(\check{\tau})}{\hat{\tau} - \check{\tau}}, \quad \dot{e} = \dot{\gamma}(\check{\tau}) - \alpha \check{\tau} \qquad [4.5]$$

where subscripts (k) and (r) have been omitted for clarity and $\dot{\gamma}(\tau)$ denotes the shear-rate given by non-linear relation [4.2] for the shear stress τ. The optimal choice (from the point of view of the variational mechanical problem) of the reference stresses $\check{\tau}_{(k)}^{(r)}$ and $\hat{\tau}_{(k)}^{(r)}$ is not straightforward and this is one reason why several extensions of the SC scheme for viscoplasticity have been proposed in the literature. Obviously, all of them reduce to the same (original) SC model in the linear case $n = 1$. Focus will be made here on the most advanced method to date, namely the "Second-Order" (SO) method [PON 02, LIU 04]. The basic idea of this method is to guide the choice of the properties of the NPLCP using a suitably designed variational principle. Furthermore, unlike the variational procedure of [PON 91], the chosen NPLCP is here of a generalized affine type, i.e. $\dot{e}_{(k)}^{(r)}$ are not required to vanish. The original procedure consists of estimating the effective stress potential $\tilde{U}$ from which the effective strain-rate can be derived, $\dot{\bar{\varepsilon}} = \partial \tilde{U} / \partial \bar{\sigma}$. The application of this method to anisotropic polycrystals, for which the form of $\tilde{U}$ is not known in advance, would require a numerical differentiation of $\tilde{U}$ which may be rather laborious. Therefore, use is made here of an approximation of the original SO formulation which aims at evaluating the effective behavior directly without having to know the effective potential, by a direct identification of the fields in the NPLCP with those of the real non-linear polycrystal. This provides slightly less accurate results than the original formulation [LIU 04], but is much more efficient from the computational point of view. The reference shear stresses now read

$$\check{\tau}_{(k)}^{(r)} = \left\langle \tau_{(k)} \right\rangle^{(r)}, \quad \hat{\tau}_{(k)}^{(r)} = \check{\tau}_{(k)}^{(r)} \pm \left[\left\langle \left(\tau_{(k)} - \check{\tau}_{(k)}^{(r)} \right)^2 \right\rangle^{(r)} \right]^{0.5}. \qquad [4.6]$$

It is worth noting that the compliance in linear relation [4.4] depends on the first *and* second moments of the phase average stress, through $\hat{\tau}_{(k)}^{(r)}$, which means that the definition of the NPLCP already captures part of the field heterogeneities in the non-linear polycrystal.

At the risk of oversimplification, the so-called "affine" (AFF) model [MAS 00] is based on linear behavior [4.4] tangent to the non-linear behavior [4.2] at the *mean* shear stress and can be understood in terms of the following relations

$$\check{\tau}_{(k)}^{(r)} = \hat{\tau}_{(k)}^{(r)} = \left\langle \tau_{(k)} \right\rangle^{(r)}, \quad \alpha_{(k)}^{(r)} = \left.\frac{\partial \dot{\gamma}}{\partial \tau}\right|_{\tau = \check{\tau}_{(k)}^{(r)}}. \qquad [4.7]$$

Thus, it does not use the intraphase heterogeneities for the construction of the NPLCP as the SO procedure does, leading to a slightly simpler numerical resolution. The limitations of this model are described in [BOR 98, MAS 00]. Generally speaking, the affine extension is known to predict an effective behavior that is too stiff, with possible violations of rigorous bounds.

Finally, the "tangent" (TGT) extension of the SC scheme [MOL 87, LEB 93] is based on the same tangent linearization [4.7] as the AFF method. However, unlike the AFF extension, this procedure takes advantage of the fact that, for power law polycrystals with a single stress exponent n, the tangent behavior [4.4] can be replaced by a secant-like relation, with $\dot{e}_{(k)}^{(r)} = 0$ and $\alpha_{(k)}^{(r)}$ replaced by $n\alpha_{(k)}^{(r)}$. A similar procedure is further applied at the macroscopic level, leading to an inconsistent combination of a secant description for the local and global behavior but a tangent analysis for the inclusion/matrix interaction [MAS 00].

4.4.2. *Results*

Figure 4.5 shows the equivalent effective stress $\bar{\sigma}_{eq}/\tau_0$ predicted by the TGT, AFF and SO extensions of the SC scheme, as a function of "cubic" system strength M_1 (still with infinite M_2), together with the static ($\boldsymbol{\sigma}(\mathbf{x}) = \bar{\boldsymbol{\sigma}}$) and Taylor ($\dot{\boldsymbol{\varepsilon}}(\mathbf{x}) = \dot{\bar{\boldsymbol{\varepsilon}}}$) bounds. Results are compared to the reference solution provided by the FFT full-field approach. First of all, it is observed that the FFT approach indicates an effective stress increasing continuously with M_1. At sufficiently large M_1 value, e.g. $M_1 > 10$, a rather simple scaling law is observed, with $\bar{\sigma}_{eq}/\tau_0$ being proportional to M_1^k, with $k \simeq 0.5$, in agreement with previous findings on other materials [NEB 00, LEB 07]. The TGT extension of the SC scheme, on the other hand, shows a saturation of $\bar{\sigma}_{eq}/\tau_0$ still at moderate values of M_1 ($\simeq 20$) which clearly departs from the reference FFT results. Since $\bar{\sigma}_{eq}/\tau_0$ remains finite when $M_1 \to \infty$, the TGT model unrealistically allows the polycrystal to deform with only three independent slip systems. It thus behaves qualitatively like the Static bound, but with a higher flow stress. As expected, the Taylor bound significantly overestimates the effective stress which simply tends to be proportional to M_1 ($k \simeq 1$). The AFF formulation provides a significantly better match to the full-field solution compared to the TGT model, at no additional numerical cost. However, the AFF flow stress increases too rapidly with M_1 ($k \simeq 0.7$). On the other hand, predictions of the SO procedure reproduce the FFT reference results almost perfectly. Unlike all other models, it predicts the correct scaling with $k \simeq 0.5$.
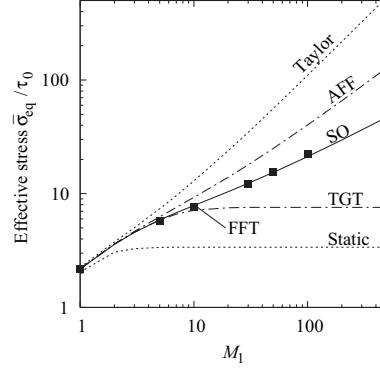
Figure 4.5. *Effect of the "cubic system" M_1 on the effective stress for several extensions of the SC scheme and compared to the reference solutions provided by the FFT full-field modeling. Static and Taylor bounds are also indicated. Here, system M_2 is not considered*

The evolution of the corresponding overall stress and strain-rate heterogeneities $\Sigma(\sigma_{eq})/\tau_0$ and $\Sigma(\dot{\varepsilon}_{eq})/\dot{\gamma}_0$, defined as

$$\Sigma(\sigma_{eq}) = \sqrt{\langle \sigma_{eq}^2 \rangle - \bar{\sigma}_{eq}^2}, \quad \Sigma(\dot{\varepsilon}_{eq}) = \sqrt{\langle \dot{\varepsilon}_{eq}^2 \rangle - \dot{\bar{\varepsilon}}_{eq}^2}, \qquad [4.8]$$

is shown in Figure 4.6. These quantities are related to the standard deviation of stress and strain-rate in the whole polycrystal. They illustrate the *overall* heterogeneities in the polycrystal, combining the field fluctuations inside the grains together with the fluctuations between different grains. It can be seen that the full-field solution predicts that stress and strain-rate heterogeneities severely increase with M_1, as already pointed out in section 4.3. Again, the TGT approach exhibits an unrealistic response, with a saturation at M_1 values as small as ~ 5–10 (note in passing that static and Taylor bounds lead to $\Sigma(\sigma_{eq}) = 0$ and $\Sigma(\dot{\varepsilon}_{eq}) = 0$, respectively, by construction). The AFF, VAR and SO estimates provide good trends, in good agreement with full-field results. Note also that the SO procedure shows an almost perfect match with the reference results for $\Sigma(\sigma_{eq})/\tau_0$.

These results suggest that 3 independent slip systems are not enough to reach a finite flow stress in olivine polycrystal. This is proved by the FFT results and correctly reproduced by the SO procedure. Thus, in the real material, some accommodation processes (such as dislocation climb or grain boundary sliding) are *necessarily* activated. The introduction of such mechanisms into the homogenization scheme requires developments that are beyond the scope of the present work. However, it is of interest to check whether 5 independent systems are really necessary. For example, simultaneous climb of **a** and **c** dislocations would ensure the olivine grains deform axially along **a** and **c**, but still not along **b**, leaving 4 independent systems at the grain scale. Therefore, we consider now the last slip system of Table 4.1 with strength M_2. This
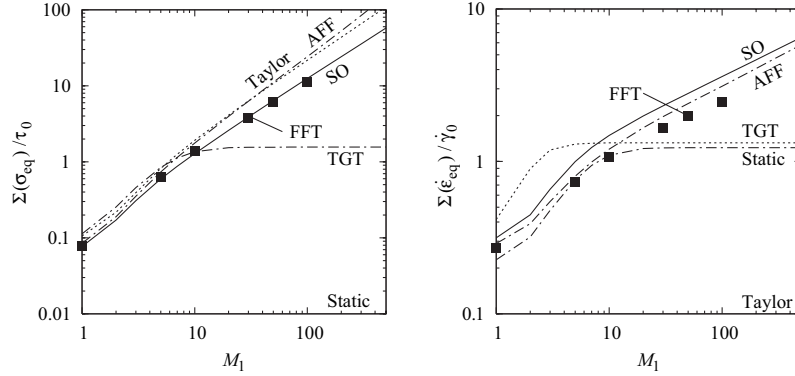
Figure 4.6. *Overall heterogeneities of (left) equivalent stress and (right) equivalent strain-rate as a function of the parameter M_1 for several extensions of the SC scheme and compared to the reference solutions provided by the FFT full-field modeling*

slip system allows axial strain along **a** and **c** only. The effective stress obtained by the SO procedure for $M_2 = 10$ and $M_2 = 50$ and different strength of the "cubic" system M_1, is shown in Figure 4.7a. Once more, the excellent behavior of the SO mean-field approach, when compared to the reference full-field solution, is remarkable. At sufficiently large M_1 values (≥ 100), a saturating behavior is observed, suggesting that olivine polycrystals can deform still as $M_1 \to \infty$, i.e. with only 4 independent slip systems. In this saturating regime[2], the evolution of the flow stress with M_2 indicates that the effective behavior of the polycrystal is largely driven by the value of M_2, even if this mechanism very poorly contributes to the overall strain (Figure 4.7b). In agreement with previous results, a scaling law with $\bar{\sigma}_{eq}$ proportional to $M_2^{0.5}$ is obtained, but now only after a large value of M_2 (≥ 100).

4.5. Concluding observations

In this study, reference solutions in term of effective behavior and field distributions have been obtained by means of the FFT full-field approach. We have observed the tremendous increase of intragranular stress and strain-rate heterogeneities as the strength of the "cubic" system M_1 increases (thus tending to leave crystals with only 3 independent slip systems). At the same time, the effective flow stress increases as $M_1^{0.5}$. Among all mean-field approaches used here, only the SO procedure is able to predict the correct trend and good quantitative match to the full-field results. This is a remarkable result. In spite of the complicated shape of the stress and strain-rate distributions occurring in an actual polycrystal, the SO approach still accurately captures

---

2. The corresponding behavior can be obtained by taking very high values of M_1, but our numerical code also converged without considering the "cubic" system at all.
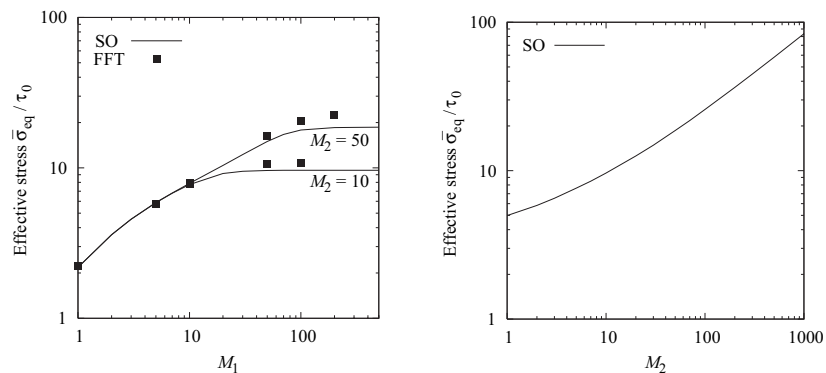
Figure 4.7. *(left) Evolution of the effective stress with respect to the flow stress of the "cubic" system M_1, for $M_2 = 10$ and $M_2 = 50$. SO and FFT predictions are compared. (right) Effective stress obtained at saturation (i.e. $M_1 \to \infty$) as function of the flow stress of the "climb" system M_2. SO predictions*

the main features of the field statistics. This success is attributed to the fact that the linearized compliances depend explicitly on the second moment of the stress. It is also worth mentioning that this procedure does not considerably increase the numerical cost when compared to the AFF estimate (generally by a factor of about 20), so that subsequent coupling with a large-scale convection model may still be tractable. The SO procedure correctly estimates the intergranular interactions and their effect on the effective behavior. We thus anticipate that this approach will be successful in bridging experimental rheological data on single- and poly-crystals, a scale transition that could not be achieved quantitatively with simpler approaches [DAW 00]. The corollary is that the SO approach, thanks to its accuracy and the limited calculation cost it requires, can be used in an inverse way to learn more about accommodation processes in olivine, by comparing numerical results to experimental data. Implications of the above results in term of deformation mechanisms and geophysical issues have been detailed in [CAS 08a]. The next step of this work is to introduce in the actual formulation the "correct" accommodation mechanisms in olivine (or at least what is actually known about them), in particular dislocation climb that has been evidenced experimentally and to account for the evolution of the slip system's strength with, for example, pressure, temperature, water fugacity, etc. Also needed for application of this work to *in situ* conditions is the consideration of other mineral phases present in the upper mantle, such as pyroxenes the volume fraction of which is $\sim 30\%$. This phase exhibiting essentially a single easy glide slip system, we may expect in peridotites (i.e. olivine-pyroxene agregates) even larger stress and strain-rate heterogenities than those obtained here, which in turn may have significant influence on dynamic recrystallization processes and subsequent influence on LPO development.

4.6. Bibliography

[BLA 07] BLACKMAN D.K., "Use of mineral physics, with geodynamic modeling and seismology, to investigate flow in the Earth's mantle", *Rep. Prog. Phys.*, vol. 70, p. 659–689, 2007.

[BOR 98] BORNERT M. and PONTE CASTAÑEDA P., "Second-order estimates of the self-consistent type for viscoplastic polycrystals", *Proc. R. Soc. Lond.*, vol. A454, p. 3035–3045, 1998.

[BOT 95] DE BOTTON G. and PONTE CASTAÑEDA P., "Variational estimates for the creep behaviour of polycrystals", *Proc. R. Soc. Lond.*, vol. A448, p. 121–142, 1995.

[CAS 08a] CASTELNAU O., BLACKMAN D.K., LEBENSOHN R.A. and PONTE CASTAÑEDA P., "Micromechanical modeling of the viscoplastic behavior of olivine", *J. Geophys. Res.*, 2008, in press.

[CAS 08b] CASTELNAU O., DUVAL P., MONTAGNAT M. and BRENNER R., "Elasto-viscoplastic micromechanical modeling of the transient creep of ice", *J. Geophys. Res.*, 2008, submitted.

[CHA 93] CHASTEL Y.B., DAWSON P.R., WENK H.-R. and BENNETT K., "Anisotropic convection with implications for the upper mantle", *JGR*, vol. 98, p. 17757–17772, 1993.

[CHR 87] CHRISTENSEN U.R., "Some geodynamical effects of anisotropy viscosity", *Geophys. J. R. Astr. Soc.*, vol. 91, p. 711–736, 1987.

[DAW 00] DAWSON P.R. and WENK H.R., "Texturing of the upper mantle convection", *Phil. Mag. A.*, vol. 80, p. 573–598, 2000.

[DUR 05] DURINCK J., LEGRIS A. and CORDIER P., "Pressure sensitivity of olivine slip systems: first-principle calculations of generalized stacking faults", *Phys. Chem. Minerals*, vol. 32, p. 646–654, 2005.

[ESH 57] ESHELBY J.D., "The determination of the elastic field of an ellipsoidal inclusion and related problems", *Proc. R. Soc. Lond.*, vol. A241, p. 376–396, 1957.

[GIL 95] GILORMINI P., "A critical evaluation for various non-linear extensions of the self-consistent model", *Proc. IUTAM Symp. on Micromechanics of Plasticity and Damage of Multiphase Materials*, Sèvres, France, Klower Academic Publishers, 1995.

[HER 54] HERSHEY A.V., "The elasticity of an isotropic aggregate of anisotropic cubic crystals", *J. Appl. Mech.*, vol. 21, p. 236–240, 1954.

[HIR 03] HIRTH G. and KOHLSTEDT D., "Rheology of the upper mantle and the wedge: a view from the experimentalists", *Geophys. Monograph*, vol. 138, p. 83–105, 2003.

[HUT 77] HUTCHINSON J.W., "Creep and plasticity of hexagonal polycrystals as related to single crystal slip", *Met. Trans.*, vol. 8A, num. 9, p. 1465–1469, 1977.

[IDI 07] IDIART M. and PONTE CASTAÑEDA P., "Field statistics in non-linear composites. I. Theory", *Proc. R. Soc. Lond.*, vol. 463, p. 183–202, 2007.

[KAM 01] KAMINSKI E. and RIBE N.M., "A kinematic model for recrystallization and texture development in olivine polycrystal", *Earth Planet. Sci. Lett.*, vol. 189, p. 253-267, 2001.

[KAR 93] KARATO S. and WU P., "Rheology of the upper mantle: a synthesis", *Science*, vol. 260, p. 771–778, 1993.

[KOH 96] KOHLSTEDT D. and ZIMMERMAN M.E., "Rheology of partially molten mantle rocks", *Annu. Rev. Earth Planet. Sci.*, vol. 24, p. 41–62, 1996.

[KRÖ 58] KRÖNER E., "Berechnung der elastischen Konstanten des Vielkristalls aus den Konstanten des Einkristalls", *Z. Physik*, vol. 151, p. 504–518, 1958.

[LEB 93] LEBENSOHN R.A. and TOMÉ C.N., "A self-consistent anisotropic approach for the simulation of plastic deformation and texture development of polycrystals: application to zirconium alloys", *Acta Metall. Mater.*, vol. 41, num. 9, p. 2611–2624, 1993.

[LEB 01] LEBENSOHN R.A., "N-site modeling of a 3D viscoplastic polycrystal using Fast Fourier Transform", *Acta Mat.*, vol. 49, p. 2723–2737, 2001.

[LEB 07] LEBENSOHN R.A., TOMÉ C.N. and PONTE CASTAÑEDA P., "Self-consistent modeling of the mechanical behavior of viscoplastic polycrystals incorporating field fluctuations", *Phil. Mag.*, vol. 87, num. 28, p. 4287–4322, 2007.

[LIU 04] LIU Y. and PONTE CASTAÑEDA P., "Second-order theory for the effective behavior and field fluctuations in viscoplastic polycrystals", *J. Mech. Phys. Solids*, vol. 52, p. 467–495, 2004.

[MAC 85] MACKWELL S.J., KOHLSTEDT D.L. and PATERSON M.S., "The role of water in the deformation of olivine single crystals", *J. Geophys. Res.*, vol. 90, p. 11319–11333, 1985.

[MAN 97] MANGENEY A., CALIFANO F. and HUTTER K., "A numerical study of anisotropic, low-Reynolds number, free surface flow for ice sheet modeling", *J. Geophys. Res.*, vol. 102, p. 22749-22764, 1997.

[MAS 00] MASSON R., BORNERT M., SUQUET P. and ZAOUI A., "An affine formulation for the prediction of the effective properties of non-linear composites and polycrystals", *J. Mech. Phys. Solids*, vol. 48, p. 1203–1226, 2000.

[MOL 87] MOLINARI A., CANOVA G.R. and AHZI S., "A self-consistent approach of the large deformation polycrystal viscoplasticity", *Acta Metall.*, vol. 35, num. 12, p. 2983–2994, 1987.

[MOU 98] MOULINEC H. and SUQUET P., "A numerical method for computing the overall response of non-linear composites with complex microstructure", *Comput. Methods Appl. Mech. Engrg.*, vol. 157, p. 69–94, 1998.

[NEB 00] NEBOZHYN M.V., GILORMINI P. and PONTE CASTAÑEDA P., "Variational self-consistent estimates for viscoplastic polycrystals with highly anisotropic grains", *C. R. Acad. Sci. Paris*, vol. 328, num. IIb, p. 11–17, 2000.

[NEB 01] NEBOZHYN M.V., GILORMINI P. and PONTE CASTAÑEDA P., "Variational self-consistent estimates for cubic viscoplastic polycrystals: the effects of grain anisotropy and shape", *J. Mech. Phys. Solids*, vol. 49, p. 313–340, 2001.

[PAR 90] PARKS D.M. and AHZI S., "Polycrystalline Plastic Deformation and Texture Evolution for Crystals Lacking Five Independent Slip Systems", *J. Mech. Phys. Solids*, vol. 38, p. 701–724, 1990.

[PON 91] PONTE CASTAÑEDA P., "The effective mechanical properties of non-linear isotropic composites", *J. Mech. Phys. Solids*, vol. 39, p. 45–71, 1991.

[PON 96] PONTE CASTAÑEDA P., "Exact second-order estimates for the effective mechanical properties of non-linear composite materials", *J. Mech. Phys. Solids*, vol. 44, p. 827–862, 1996.

[PON 98] PONTE CASTAÑEDA P. and SUQUET P., "Nonlinear composites", *Adv. Appl. Mech.*, vol. 34, p. 171–302, 1998.

[PON 02] PONTE CASTAÑEDA P., "Second-order homogenization estimates for non-linear composites incorporating field fluctuations. I – Theory", *J. Mech. Phys. Solids*, vol. 50, p. 737–757, 2002.

[RAT 07] RATERRON P., CHEN J., LI L., WEIDNER D. and CORDIER P., "Pressure-induced slip-system transition in forsterite: single-crystal rheological properties at mantle pressure and temperature", *Am. Mineral.*, vol. 92, p. 1436–1445, 2007.

[TOM 00] TOMMASI A., MAINPRICE D., CANOVA G. and CHASTEL Y., "Viscoplastic self-consistent and equilibrium-based modeling of olivine lattice preferred orientations: implications for the upper mantle seismic anisotropy", *J. Geophys. Res.*, vol. 105, p. 7893–7908, 2000.

[WEN 99] WENK H.R. and TOMÉ C.N., "Modelling dynamic recrystallization of olivine aggregates deformed in simple shear", *J. Geophys. Res.*, vol. 104, p. 25513–25527, 1999.

[ZHA 95] ZHANG S. and KARATO S., "Lattice prefered orientation of olivine aggragates deformed in simple shear", *Nature*, vol. 375, p. 774–777, 1995.